Fabrication of a three-dimensional micro-manipulator by laser irradiation and electrochemical techniques and the effect of electrolytes on its performance

T. Kikuchi*, Y. Akiyama, M. Ueda, M. Sakairi, and H. Takahashi

Graduate School of Engineering, Hokkaido University,

N13, W8, Kita-Ku, Sapporo, Japan

Corresponding author: T. Kikuchi

TEL: +81-11-706-7112

FAX: +81-11-706-7881

E-mail: kiku@elechem1-mc.eng.hokudai.ac.jp

Abstract

Ribbon type and three-dimensional micro-actuators, consisting of three-layer structure of acrylic acid resin / Au / polypyrrole, were fabricated by aluminum anodizing, laser irradiation, and electrochemical techniques, and their performance was examined. Anodized aluminum specimens were irradiated with a pulsed Nd-YAG laser to remove anodic oxide films locally, and then an Au layer was deposited at the

area where film had been removed. The subsequent electrophoretic deposition of acrylic acid resin on the Au layer, dissolution of anodic oxide film and the metal substrate, and deposition of polypyrrole on backside of Au layer by electro-polymerization enabled the fabrication of a three-layer actuator. Cyclic voltammetry of the ribbon type actuator in different electrolyte solutions showed that redox reactions of polypyrrole is accompanied with doping and dedoping of hydrated cations, and that the redox reaction strongly depends on the valency of cations in the solutions. The three-dimensional micro-actuator showed good performance as a manipulator, gripping and moving objects of several mg in solutions.

Key words: Aluminum; Conducing polymer; Micro-actuator; Manipulator; MEMS

1. INTRODUCTION

Micro-actuators based on conducting polymers such as polypyrrole (PPy), polyaniline, and polythiophene have been widely investigated in the field of micro-electromechanical systems (MEMS) and bio-mimetic devices [1-8]. The

principle of actuators with a bi-layer structure of conducting polymer and metal layer (or non-conducting organic layer) is based on the volume expansion of the conducting polymer by doping ions from electrolyte solutions into the polymer layer and on a volume shrinkage by dedoping. The doping and dedoping of ions can be achieved by changing the potential of the bi-layer structure, because the metal layer or non-conducting organic layer does not change in volume. Micrometer and nanometer scale actuators with a planar structure have been fabricated by photolithography with a resist pattern and selective polymer-film deposition, but micro- or nano-actuators with three-dimensional (3D) structure have not been reported. This is because 3D micro-actuators with non-planar shapes cannot be fabricated using photolithography, due to difficulties in the preparation of non-planar photo-masks with a uniform thickness, and uniform light irradiation without shade.

The authors have been developing a new method for fabricating micro-actuators using laser irradiation and electrochemical techniques such as anodizing, electroplating, and electro-polymerization [9]. In this technique, aluminum specimens covered with anodic oxide films are irradiated with a pulsed Nd-YAG laser to remove the oxide film,

and then a metal layer is deposited by electroplating at the laser-irradiated area. After dissolving the aluminum substrate and the oxide film, one side of the metal layer is covered with nitrocellulose, and the other side is covered with PPy by electro-polymerization of the pyrrole. A ribbon-shaped microstructure with three layers; nitrocellulose, metal, and PPy, showed a stable swing motion when varying the potential of the actuator in solutions, although the actuator was found to display distorted motion when there was non-uniformities in the nitrocellulose layer.

The authors also developed a technique for the fabrication of 3D metal microstructures by rotation, moving-up, and moving-down of the 3D-shaped aluminum specimen during laser irradiation [10-14], and here have attempted to combine the techniques of micro-actuator fabrication with those of 3D microstructure fabrication to develop a new type of actuator, which shows no distortion in the motion.

The present investigation reports the fabrication of a ribbon type and 3D micro-manipulator consisting of three layers, PPy, Au, and acrylic acid resin, by anodizing of aluminum, laser irradiation, Au / acrylic resin electro-deposition, and PPy deposition by electro-polymerization.

2. EXPERIMENTAL

2.1 Specimens and pretreatment

Highly pure aluminum plate (99.99 wt%, 0.35 mm thick, 20 mm x 18 mm with a handle, Nippon Light Metal) and commercial aluminum tube (99.5 wt%, 1.6 mm inner diameter, 2.0 mm outer diameter, 35 mm long, Nilaco) were used as specimens. The specimens were degreased ultrasonically in C_2H_5OH solution, and then electropolished in 13.6 kmol m^{-3} CH_3COOH / 2.56 kmol m^{-3} $HClO_4$ solution with a constant voltage of 28 V at 280 K. Electropolished specimens were anodized in 0.22 kmol m^{-3} $(COOH)_2$ solution at 293 K for 30 min with a constant current density of 100 A/m^2 to form 9 μm thick porous type oxide film (Fig. 1a). After anodizing, the specimens were immersed in 0.029 kmol m^{-3} alizarin red S dyeing solution at 323 K for 5 min, and then boiled in doubly distilled water for 15 min to seal the pores.

2.2 Fabrication of ribbon and 3D actuators

The anodized specimens were immersed in a commercial Au electroplating solution (ECF-60, pH = 9.44, N. E. CHEMCAT) at 293 K, and then irradiated with a

Pulsed Nd-YAG laser (Fig. 1b). Details of the laser irradiation setup have been shown elsewhere [10]. The specimens were set in a defocused position, 5 mm from the focal plane of a laser beam that had passed through a beam splitter, an iris diaphragm, a convex lens with 60 mm focal length, and a quartz window. The laser beam has 532 nm wavelength (second harmonic generation), 8 ns pulse width, 10 Hz frequency, and < 0.5 mrad beam divergence (full angle). For the fabrication of the ribbon type actuator, planar specimens were moved at 200 μm/s with a PC-controlled XYZ-stage to remove the oxide film at a rectangular area of 14 mm x 0.2 mm from the aluminum substrate. In the 3D actuator fabrication, columnar specimens were rotated at 10.0 degree/s with a θ-stage in addition to the up-and-down movement with the XYZ-stage to make the network pattern with four projections (fingers).

The laser-irradiated specimens were, then, polarized cathodically for 30 min at constant potential of -0.7 V and 293 K to deposit a 5 μm thick Au metal layer on the area where film had been removed by the laser irradiation (Fig. 1c). A Pt plate was used as the counter electrode and a saturated KCl-Ag/AgCl electrode as the reference electrode for the Au electroplating. The Au electroplated specimens were immersed in

an acrylic acid and melamine oligomer solution (Honny Bright, acrylic acid resin : melamine resin = 72 : 28, Honny Chemicals) at room temperature, and then polarized anodically for 60 s at a constant voltage of 10 V to deposit an acrylic acid / melamine resin layer on the Au layer (Fig. 1d). After electrophoretic deposition, heat treatment was carried out for 30 min at 403 K to polymerize the resin completely. The specimens were then immersed in 3 kmol m^{-3} NaOH solution at room temperature for 120 min to dissolve the aluminum substrate and the anodic oxide film to obtain a free-standing bi-layer structure of Au / acrylic acid resin (Fig. 1e).

For the PPy film deposition, the bi-layer structures were connected with a copper wire using Dotite electro-conductive silver paste, and immersed in 0.1 kmol m^{-3} sodium dodecylbenzenesulfonate (NaDBS) / 0.2 kmol m^{-3} pyrrole solution at 293 K. They were then polarized anodically for 30 min at a constant potential of 0.56 V (vs. Ag/AgCl) to deposit 20 μm thick PPy film on the Au layer side that had been exposed to the solution by the dissolution of the metal substrate (Fig. 1f). These successive steps, anodizing, laser irradiation, local Au deposition, local acrylic acid resin deposition, heat treatment, and pyrrole electro-polymerization enabled a successful fabrication of

ribbon-type and 3D actuators, consisting of three layers, acrylic acid resin / Au / PPy.

2.3 Cyclic voltammetry and evaluation of actuator performance

Cyclic voltamograms of the ribbon type microstructures were examined in 0.1 kmol m^{-3} solutions of NaDBS, LiCl, NaCl, $MgCl_2$, $CaCl_2$, and $AlCl_3$ at a potential scanning rate of 5 mV/s between 0.3 and -0.8 V (vs. Ag/AgCl) at room temperature. The platinum plate was used as the counter electrode. Motion of the 14 mm long ribbon microstructures was recorded on a video camera during the potential scanning, and movement of the ribbon actuator was established by noting the free-end positions at 0 V and –0.8 V (vs. Ag / AgCl).

The performance of the 3D actuator as a micro-manipulator was established by gripping and lifting a mulite cylinder ($3Al_2O_3$ $2SiO_2$, 0.5 mm inner diameter, 1.5 mm outer diameter, 2.1 mm long, 6.5 mg) in 0.1 kmol m^{-3} NaDBS solution. The platinum plate was used as the counter electrode, and the Ag / AgCl electrode was used as the reference electrode. The potentials of the 3D actuator were applied at 0 V and -0.8 V (vs. Ag / AgCl) by potential step control.

3. RESULTS AND DISCUSSION

3.1 Cyclic voltammograms of ribbon actuator in various solutions

Fig. 2 shows the cyclic voltammograms of the ribbon type actuator in 0.1 kmol m^{-3} NaDBS solution at 5, 200, and 400 cycles. The cyclic voltammograms show similar behaviors independent of number of repeated cycles, indicating a relatively large current over the potential region examined, with two low current peaks: a reduction current peak at –0.6 V and an oxidation current peak at –0.4 V. The complementary redox current peaks correspond to the redox reaction of PPy, as shown in equation 1 [9]

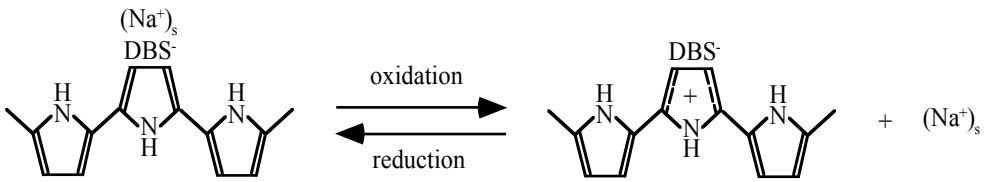

(1)

Dedoping of hydrated Na^+ ions, $(Na^+)_h$, is accompanied by PPy oxidation and the doping of $(Na^+)_h$ with PPy reduction. It is clear from Fig. 2 that the doping and dedoping of $(Na^+)_h$ is stable until 400 cycles and occurs over the potential regions examined as well as at the redox current peak potentials.

Fig. 3 shows cyclic voltammograms of the ribbon type actuator in 0.1 kmol m^{-3} NaDBS (solid line), 0.1 kmol m^{-3}-NaCl (dotted line), and 0.1 kmol m^{-3}-LiCl (chained

line) solutions at 5 cycles. The cyclic voltamograms in NaCl and LiCl solutions are similar to the cyclic voltammogram in the NaDBS solution, indicating oxidation / reduction peaks at –0.4 V / -0.6 V, respectively. It can be seen from Fig. 3 that the manner of doping and dedoping of $(Na^+)_h$ is similar to that of $(Li^+)_h$, and that doping and dedoping of anions is negligibly small. The absence of doping and dedoping of anions in this investigation may be explained by the fact that the relatively large DBS^- ions are included in the PPy matrix.

Fig. 4 shows the cyclic voltammograms of the ribbon type actuator in 0.1 M $MgCl_2$ (solid line) and in 0.1 M $CaCl_2$ (dotted line) solutions. In the $MgCl_2$ solution, there is a sharp reduction current peak at –0.45 V and two gentle oxidation current peaks at –0.35 and –0.1 V, while in the $CaCl_2$ solution, there is an oxidation current peak at –0.7 V and two reduction current peaks at –0.5 and –0.1 V. This suggests that cations are doped in one step in $MgCl_2$ and $CaCl_2$ solutions and that dedoping takes place in two parallel steps [15], and the higher over potential shows doping of $(Ca^{2+})_h$ is much harder than with $(Mg^{2+})_h$. Comparing Fig. 4 with Fig. 3 shows that the current over the potential region examined, except for the peak regions, in solutions containing

divalent cations (Mg^{2+} and Ca^{2+}) is smaller than that in solutions containing monovalent cations (Li^{+} and Na^{+}), and that divalent cation solutions show higher and sharper reduction peaks than monovalent cation solutions. Hence, doping of hydrated $(Mg^{2+})_h$ and $(Ca^{2+})_h$ occurs mainly at the reduction current peak potentials, unlike the situation in monovalent cation solutions.

Fig. 5 shows the cyclic voltammogram of the ribbon type actuator in 0.1 kmol m^{-3} $AlCl_3$ solution. The current, i, shows low values over the whole of the potential region between -0.8 V to 0.3 V without any redox peaks. This suggests that doping and dedoping of hydrated Al^{3+} ions, $(Al^{3+})_h$, is much more difficult than with monovalent cations, $(Na^{+})_h$ and $(Li^{+})_h$, and divalent cations, $(Mg^{2+})_h$ and $(Ca^{2+})_h$. The mechanism of doping and dedoping of cations will be discussed next.

3.2 Effect of cation valencies on the motion of the ribbon type actuator

Fig. 6 shows superimposed photographs of the motion of the ribbon type actuator in 0.1 M $CaCl_2$ solution with the potential of the actuator at a) 0 V and at b) -0.8 V. The photograph in Fig. 6 superimposes photos taken at 0 and –0.8 V, and shows a side view of the ribbon consisting of a PPy layer (right), an Au layer (middle), and an acrylic

resin layer (left). It can be seen from Fig. 6 that the 14 mm long ribbon bends to the right when the potential is changed from E = 0 V to E = -0.8 V, and that the distance of movement of the ribbon end, d, is 1.77 mm. The potential change from -0.8 to 0 V returns the ribbon to the initial position. The motion of the ribbon type actuator is due to an expansion of PPy by $(Ca^{2+})_h$ doping during cathodic polarization, and a shrinkage of PPy by $(Ca^{2+})_h$ dedoping during anodic polarization. The distance of movement, d, in 0.1 kmol m^{-3} solutions of NaCl, NaDBS, LiCl, $MgCl_2$, $CaCl_2$, and $AlCl_3$ between 0 and –0.8 V are listed in the second column of Table 1; the distance, d, decreases in the order of NaCl > NaDBS > LiCl > $CaCl_2$ > $MgCl_2$, >> $AlCl_3$ solutions (near absence of movement). The third column of Table 1 shows the amount of anodic charge, Q_a, and cathodic charge, Q_c, obtained in the cyclic voltammetry between –0.8 V and 0.3 V (see Figs. 2, 3, and 4). The values of Q_c are larger than Q_a in all solutions, suggesting that a charge related to oxygen reduction is included in Q_c during the measurement of the cyclic voltammograms in the air-exposed solutions.

The 4th column of Table 1 indicates the specific molar amounts, M_s, of dedoped cations during the anodic current cycles, normalized by the value in the LiCl solution.

The specific molar amount, M_s, can be expressed by the following equation

$$M_s = (Q_a / z) / Q_{a,Li} \qquad (2)$$

where $Q_{a,Li}$ is the amount of anodic charge in the LiCl solution (= 677 C), and z is the valency of the cations. The M_s value decreases in the order NaCl, NaDBS > LiCl > $MgCl_2$ > $CaCl_2$ >> $AlCl_3$. The order of decrease in M_s is very similar to that in the distance of movement, d, of the actuator (2nd column of Table 1). This strongly suggests that the motion of the actuator depends on the molar amount of doped / dedoped cations; the distance of movement increasing with the doped molar amounts.

A comparison of the 1st and 4th columns in Table 1 shows that more mono-valent cations, $Na^+$and Li^+, are doped into PPy than divalent cations, Ca^{2+} and Mg^{2+}, and that trivalent cations, Al^{3+}, are not doped. This may be because cations are present as hydrated ions in the solution [16], and hydrated monovalent cations have a smaller water sheath than divalent and trivalent cations. Higher valent cations with smaller diameters attract more water molecules, leading to the formation of the largest water sheath around Al^{3+}, a large sheath around Mg^{2+} and Ca^{2+}, and the smallest sheath around Li^+ and Na^+ ions. The hydrated Al^{3+} may be larger than the channel diameter in the

PPy matrix, showing no redox current peaks and zero moving distance. The two step dedoping processes in $MgCl_2$ and $CaCl_2$ solutions could be due to different lengths or diameters of channels, providing easy and less easy passageways. The more negative reduction current peak in $CaCl_2$ solution than in $MgCl_2$, can be explained by the differences in the size of the hydrated cations, the hydrated Ca^{2+} ions with a larger water sheath may have more difficulty in doping than the smaller of hydrated Mg^{2+}, resulting in higher overpotentials.

3.3 Motion of the 3D micro-manipulator

Fig. 7a is a photograph of an Au micro-pattern fabricated on a 2 mm diameter aluminum tube, after anodizing, laser irradiation, and Au electroplating (see Fig. 1a – 1c). In Fig. 7a, the light colored spiral and straight lines pattern at the center part of the aluminum tube corresponds to the Au-deposited area, and the gray areas to the parts covered with anodic oxide film. The spiral and the horizontal straight line of the Au micro-pattern have a 120 μm line width. Fig. 7b is a photograph of the three-layer microstructure obtained after electrophoretic deposition, lifting off, and PPy electro-polymerization (see Fig. 1d – 1f). Here, the microstructure consists of PPy

(inner layer), Au (middle layer), and acrylic resin (outer layer). The cylindrical 2 mm diameter network microstructure is connected to a copper wire (left), it has 4 fingers with 3 mm length extending beyond the spiral network. Fig. 7b clearly shows that a micro-manipulator with 4 fingers can be manufactured with the process described here.

Fig. 8 shows photographs illustrating the movement of the micro-manipulator achieved by changing the applied potential from a) -0.8 to b) 0 (at the time of the change) and c) 0 V (1 min after the change) in 0.1 M NaDBS solution. At E = -0.8 V (Fig. 8a), the 4 fingers of the microstructure point in the direction towards the outside of the microstructure, while, just after switching to E = 0 V (Fig. 8b), the fingers bend towards the inside, and the free ends of the fingers move to touch each other after keeping the potential at E = 0 V (Fig. 8c) for 1 min. Reversing the potential change from 0 to -0.8 V returned the fingers to the shape in Fig. 8a.

Fig. 9 shows photographs of the performance of the microstructure as a micro-manipulator in 0.1 kmol m^{-3} NaDBS solution. In Fig. 9a, there is a 1.5 mm diameter and 2.1 mm long mulite cylinder (6.5 mg) at the bottom of an electrolytic cell under the micro-manipulator; the four fingers of the manipulator are open with the

potential at –0.8 V. In Fig. 9b the micro-manipulator has been moved downwards and grips the cylinder; here the potential of the micro-manipulator is at E = 0 V. In Fig. 9c the manipulator has been moved upwards, holding the cylinder.

In summary, 3D micro-actuators were fabricated by successive procedures of aluminum anodizing, laser irradiation, and Au / acrylic resin / PPy electrodeposition, and no distorted motion of the micro-manipulator fingers was observed. Electrophoretic deposition of acrylic resin is considered to enable the no distorted motion because of the uniform film thickness. The micro-manipulator in the present investigation is difficult to fabricate by photolithography, and the technique described here the feasibility in medicine, biotechnology, and microelectromechanical systems (MEMS). In these applications, it is important to fabricate smaller actuators with sub-millimeter size. The authors have already succeeded in micro-patterning with 5 μm line width on aluminum substrate [17]. The sub-millimeter size actuator can be fabricated with smaller diameter aluminum tubes by the micro-patterning techniques described above, although crack formation during anodizing may confine the thickness of the PPy layer [10]. More precise and smaller actuators may be fabricated by

choosing the optimal fabrication condition.

4. CONCLUSIONS

The following conclusions may be drawn from the experiments reported above.

(1) Ribbon type and 3D micro-actuators with PPy / Au / acrylic acd resin three-layer structures can be successfully fabricated by anodizing, laser irradiation, Au electroplating, acrylic ace resin electrophoretic deposition, aluminum substrate and oxide film dissolution, and PPy electro-polymerization.

(2) Ribbon type micro-manipulators can be activated by applying and changing potentials, here from –0.8 to 0 V, repeatedly. The moving distance of the ribbon type micro-actuator components depends strongly on the valency of the cations in solution: monovalent cations (Li^+, Na^+) > divalent cations (Mg^{2+}, Ca^{2+}) > trivalent cations (Al^{3+}, little or no movement). The motion can be explained by a volume change due to the doping and dedoping of hydrated cations into / from the PPy matrix.

(3) The three-dimensional micro-actuator can be used as a manipulator for gripping and transferring small components.

References

1) T. F. Otero, H. Grande, and J. Rodriguez, Synth. Met. 83 (1996) 205.

2) T. F. Otero, I. Cantero, and H. Grande, Elechtrochim. Acta 44 (1999) 2053.

3) A. S. Hutchison, T. W. Lewis, S. E. Moulton, G. M. Spinks, and G. G. Wallace, Synth. Met. 113 (2000) 121.

4) T. F. Otero and I. Boyano, J. Phys. Chem. B107 (2003) 6730.

5) J. W. Paquette, K. J. Kim, D. Kim, Sens. Actuators A118 (2005) 135.

6) J. H. Lee, J. H. Lee, J. D. Nam, H. Choi, K. Jung, J. W. Jeon, Y. K. Lee, K. J. Kim, and Y. Tak, Sensors and Actuators A118 (2005) 98.

7) S. Maw, E. Smela, K. Yoshida, and R. B. Stein, Synth. Met. 155 (2005) 18.

8) G. Han and G. Shi, Sensors and Actuators B113 (2006) 259.

9) Y. Akiyama, T. Kikuchi, M. Ueda, M. Iida, M. Sakairi, and H. Takahashi, Electrochim. Acta 51 (2006) 4834

10) T. Kikuchi, M. Sakairi, and H. Takahashi, J. Electrochem. Soc. 150 (2003) C567

11) T. Kikuchi, H. Takahashi, and T. Maruko, Electrochim. Acta. in press (Elsevier,

Science Direct)

12) S. Z. Chu, M. Sakairi, H. Takahashi, K. Shimamura, and Y. Abe, J. Electrochem. Soc. 147 (2000) 2182

13) T. Kikuchi, S. Z. Chu, S. Jonishi, M. Sakairi, and H. Takahashi, Electrochim. Acta 47 (2001) 225

14) T. Kikuchi, M. Sakairi, H. Takahashi, Y. Abe, and N. Katayama, J. Electrochem. Soc. 148 (2001) C740

15) M. R. Gandhi, P. Murray, G. M. Spinks, and G. G. Wallace, Synth. Metals 73 (1995) 247

16) S. Skaarup, K. West, L. M. W. K. Gunaratne, K. P. Vidanapathirana, and M. A. Careem, Solid State Ionics 136-137 (2000) 577

17) T. Kikuchi, M. Sakairi, H. Takahashi, Y. Abe, and N. Katayama, Surf. Coat. Technol. 169-170C (2003) 199

Captions

Table 1 Moving distance of ribbon type micro-actuator, d, the amount of anodic and cathodic charge, Q_a and Q_c in cyclic voltammetry between –0.8 and 0.3 V, and specific molar amounts of doped cations, M_s, in 0.1 kmol m^{-3} solutions of LiCl, NaCl, NaDBS, $MgCl_2$, $CaCl_2$, and $AlCl_3$.

Fig. 1 Steps in the fabrication of the PPy / Au / acrylic resin three-layer microstructure; a) anodizing, b) laser irradiation, c) – d) Au / acrylic resin electrodeposition, e) aluminum and oxide film dissolution, and f) PPy electro-polymerization.

Fig. 2 Cyclic voltammograms of the ribbon type actuator in 0.1 kmol m^{-3} NaDBS solution at 5, 200, and 400 cycles.

Fig. 3 Cyclic voltammograms of the ribbon type actuator in 0.1 kmol m^{-3} solutions: NaDBS, NaCl, and LiCl.

Fig. 4 Cyclic voltammograms of the ribbon type actuator in 0.1 kmol m^{-3} solutions of $MgCl_2$ and $CaCl_2$.

Fig. 5 Cyclic voltammogram of ribbon type actuator in 0.1 M $AlCl_3$ solution.

Fig. 6 Superimposed video images illustrating the bending motion of the ribbon type

micro-actuator in $CaCl_2$ solution. Images obtained at a) E = 0 V and b) -0.8 V are superimposed.

Fig. 7 Optical micrographs of a) Au micro-pattern on an aluminum tube after anodizing, laser irradiation, and Au electrodeposition and b) three-layer micro-manipulator after acrylic acid resin electrodeposition, aluminum and oxide film dissolution, and PPy electrolytic polymerization.

Fig. 8 Video images illustrating the motion of the 3D micro-manipulator in 0.1 M NaDBS solution at a) -0.8 V, b) just after changing to 0 V, and c) 1 min after changing to 0 V.

Fig. 9 Video images illustrating the motion of the 3D micro-manipulator gripping a ceramics cylinder in 0.1 M NaDBS solution: a) opening the fingers at -0.8 V, b) holding the cylinder at 0 V, and c) lifting the cylinder at 0 V.

Table 1

Ion species	Moving distance, d / mm	Anodic charge, Q_a / C	Cathodic charge, Q_c / C	Ratio of number of doped cations, M_s
Li^+ (Cl^-)	4.74	677	1552	1.00
Na^+ (Cl^-)	5.39	883	1713	1.30
Na^+ (DBS^-)	4.86	933	1576	1.38
Mg^{2+} (Cl^-)$_2$	1.41	1007	1354	0.74
Ca^{2+} (Cl^-)$_2$	1.77	697	1304	0.51
Al^{3+} (Cl^-)$_3$	0	81	514	0.04

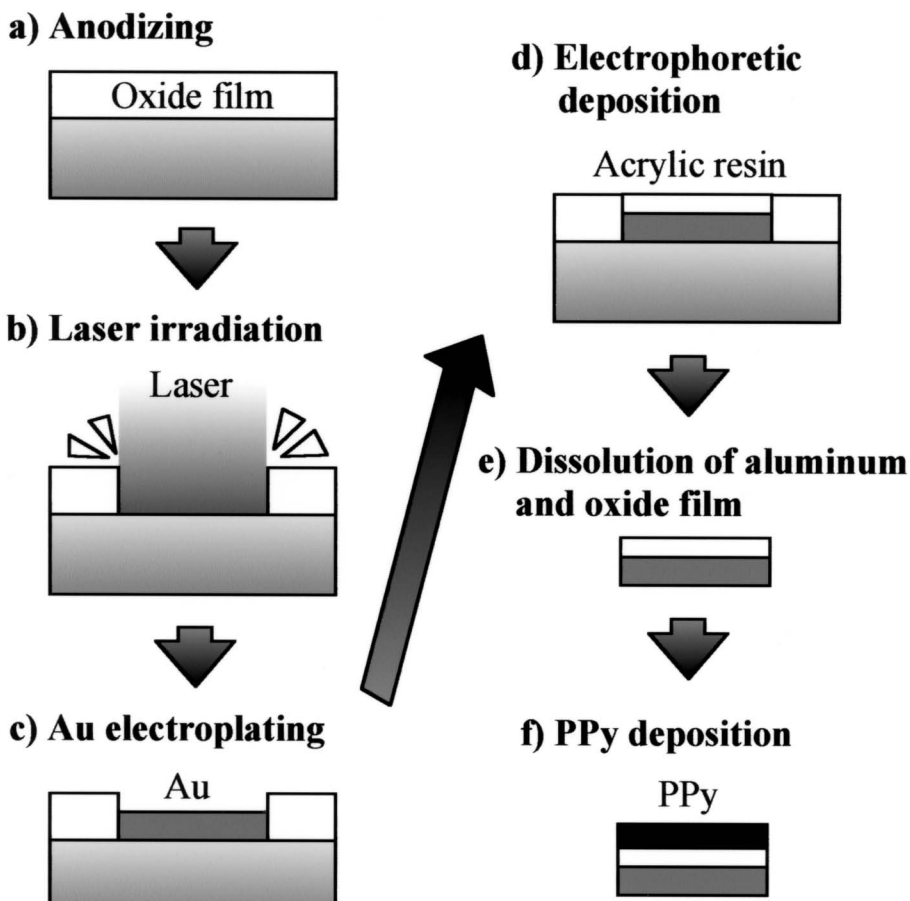
a) Anodizing
Oxide film
b) Laser irradiation
Laser
c) Au electroplating
Au
d) Electrophoretic deposition
Acrylic resin
e) Dissolution of aluminum and oxide film
f) PPy deposition
PPy

Fig. 1

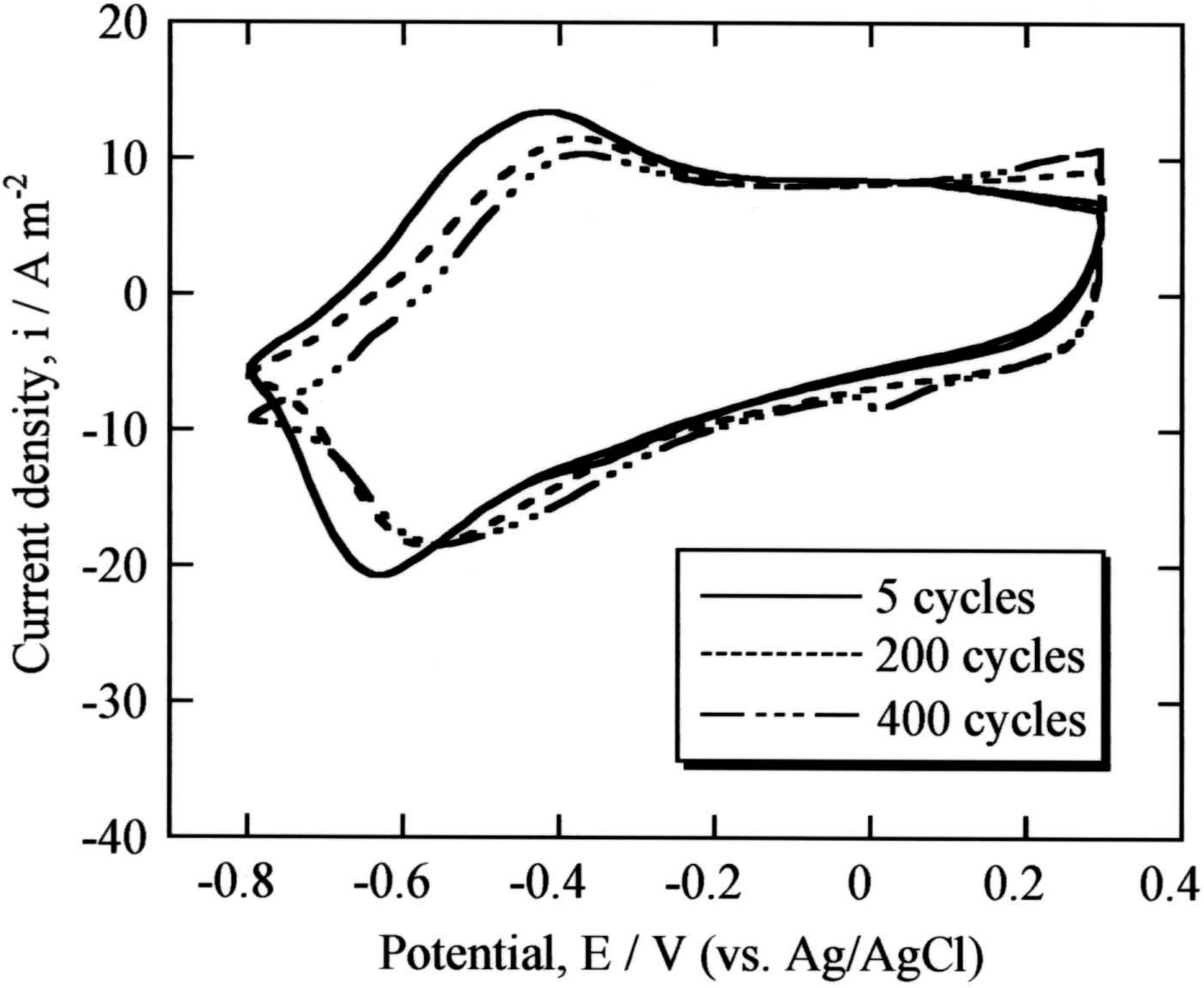
20
10
0
-10
-20
-30
-40
-0.8
-0.6
-0.4
-0.2
0
0.2
0.4
Current density, i / A m-2
Potential, E / V (vs. Ag/AgCl)
5 cycles
200 cycles
400 cycles

Fig. 2

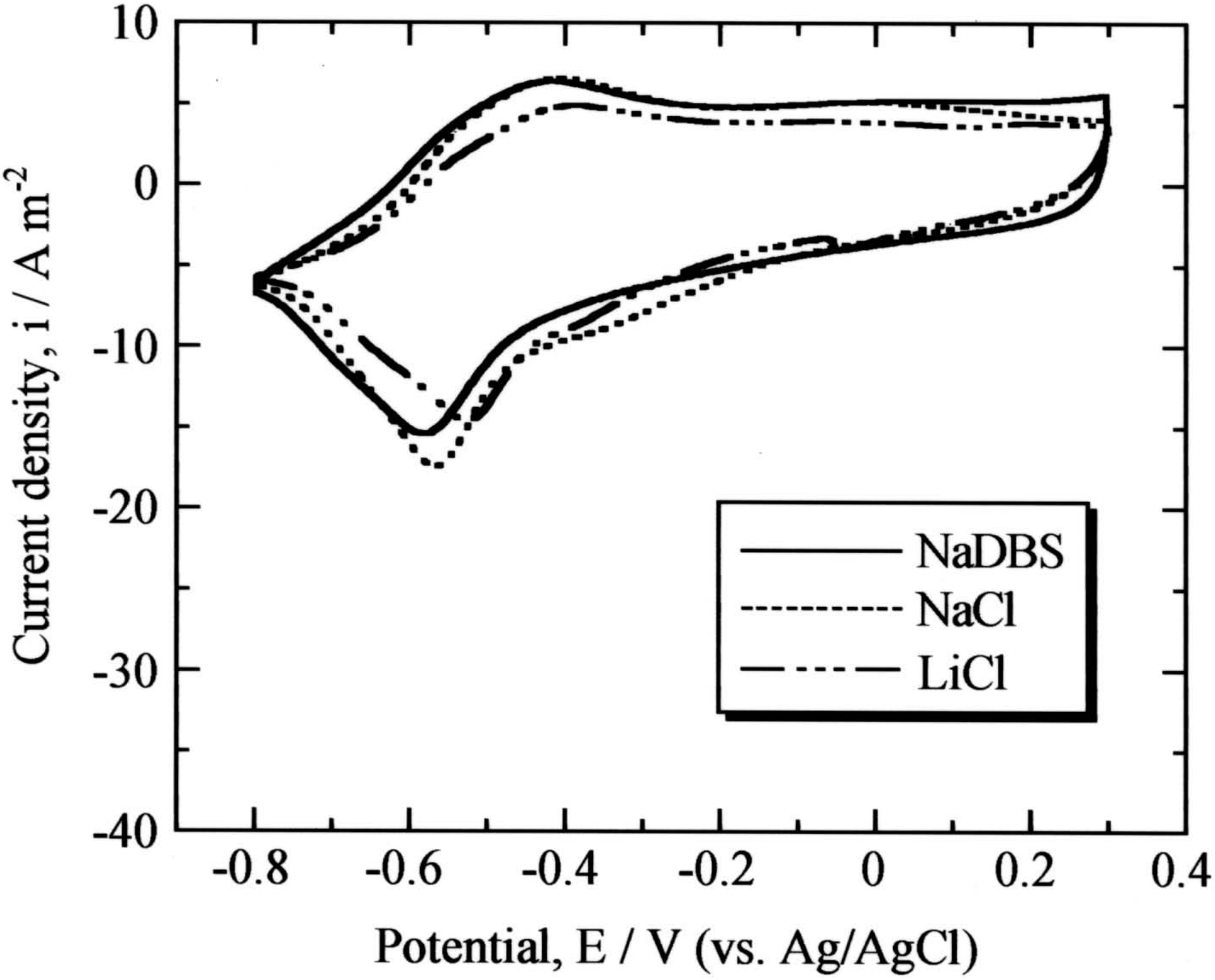
10
0
-10
-20
-30
-40
-0.8
-0.6
-0.4
-0.2
0
0.2
0.4
Current density, i / A m-2
Potential, E / V (vs. Ag/AgCl)
NaDBS
NaCl
LiCl

Fig. 3

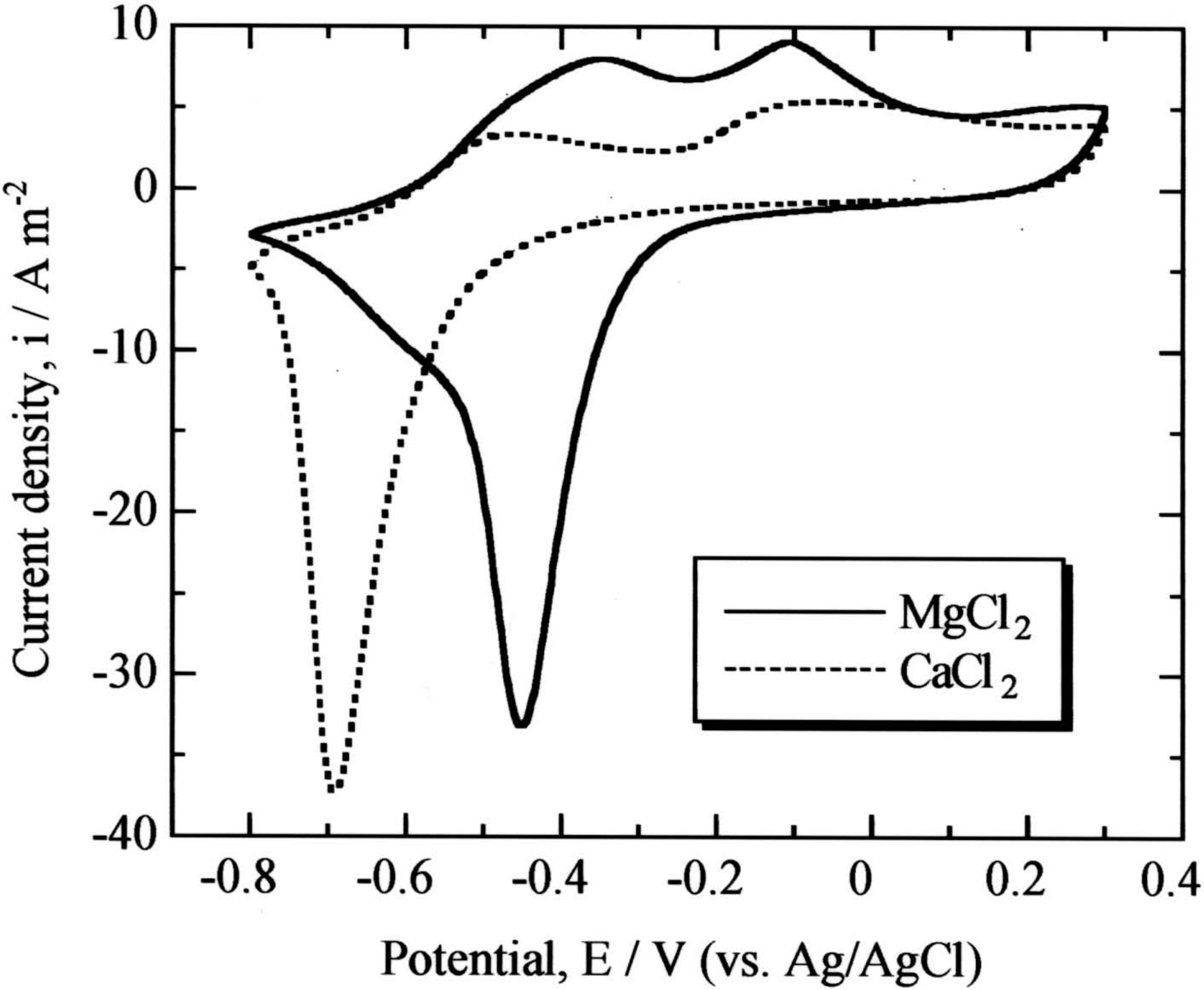
10
0
-10
-20
-30
-40
-0.8
-0.6
-0.4
-0.2
0
0.2
0.4
Current density, i / A m-2
Potential, E / V (vs. Ag/AgCl)
MgCl2
CaCl2

Fig. 4

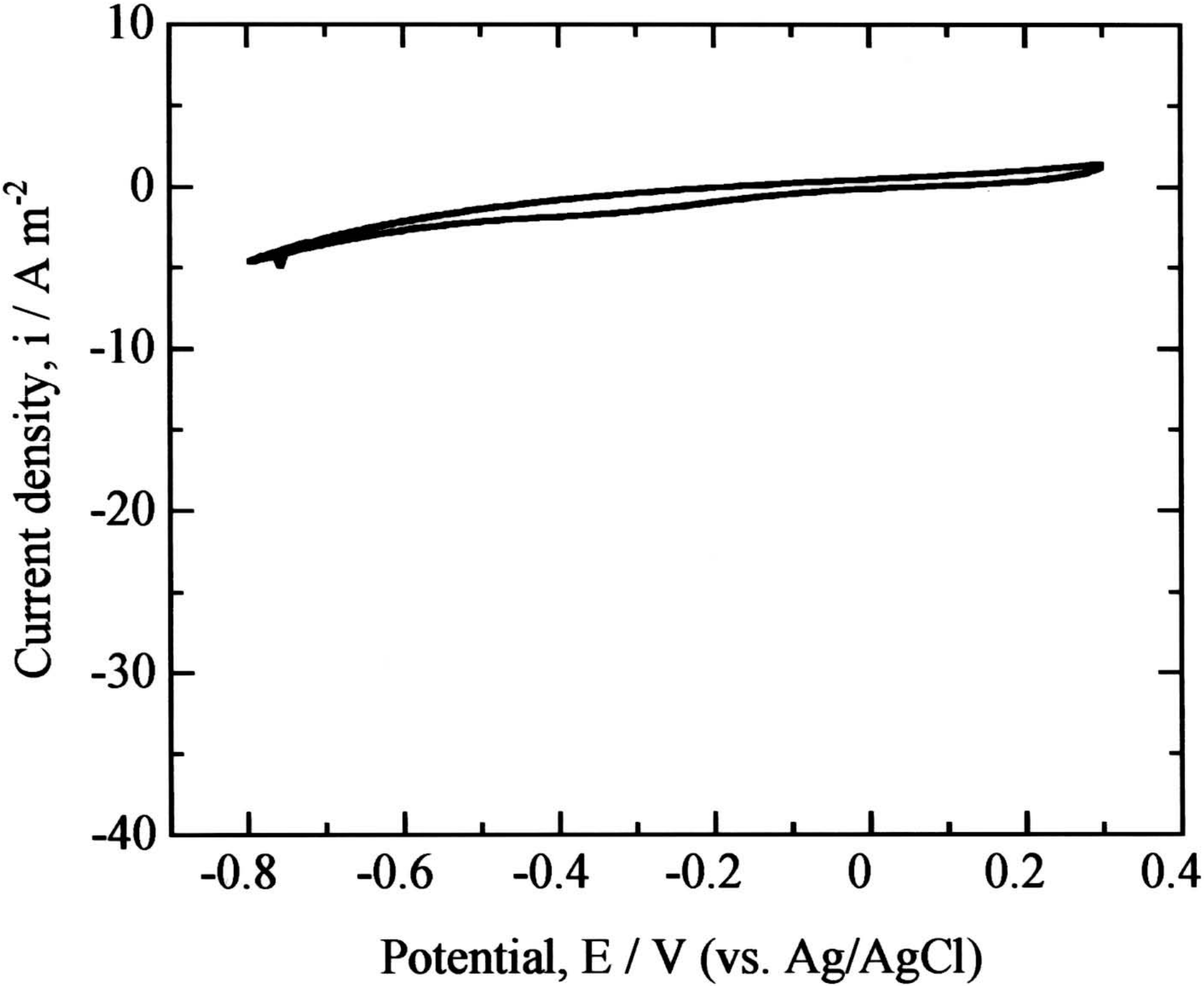
10
0
-10
-20
-30
-40
-0.8
-0.6
-0.4
-0.2
0
0.2
0.4
Current density, i / A m-2
Potential, E / V (vs. Ag/AgCl)

Fig. 5

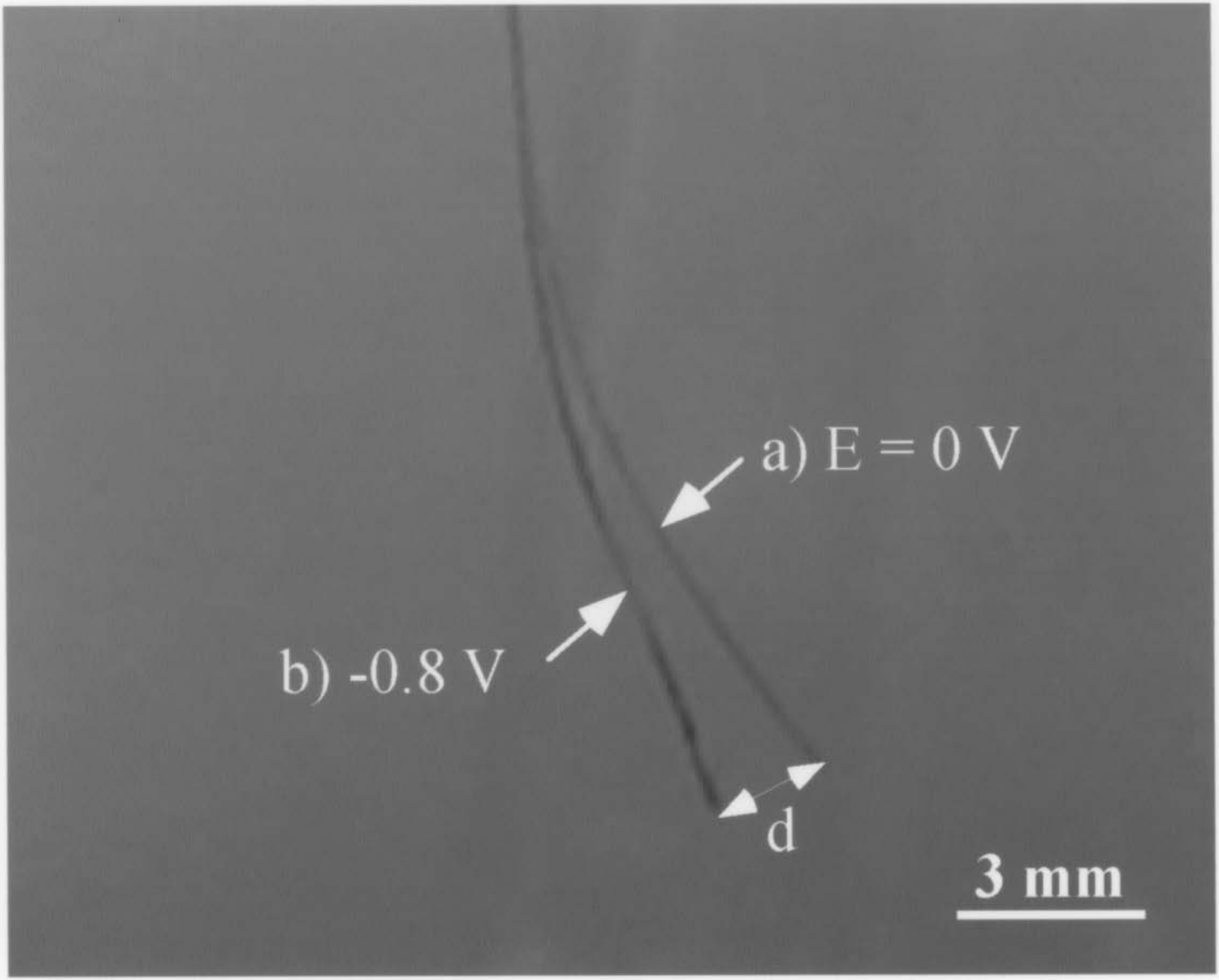

Fig. 6

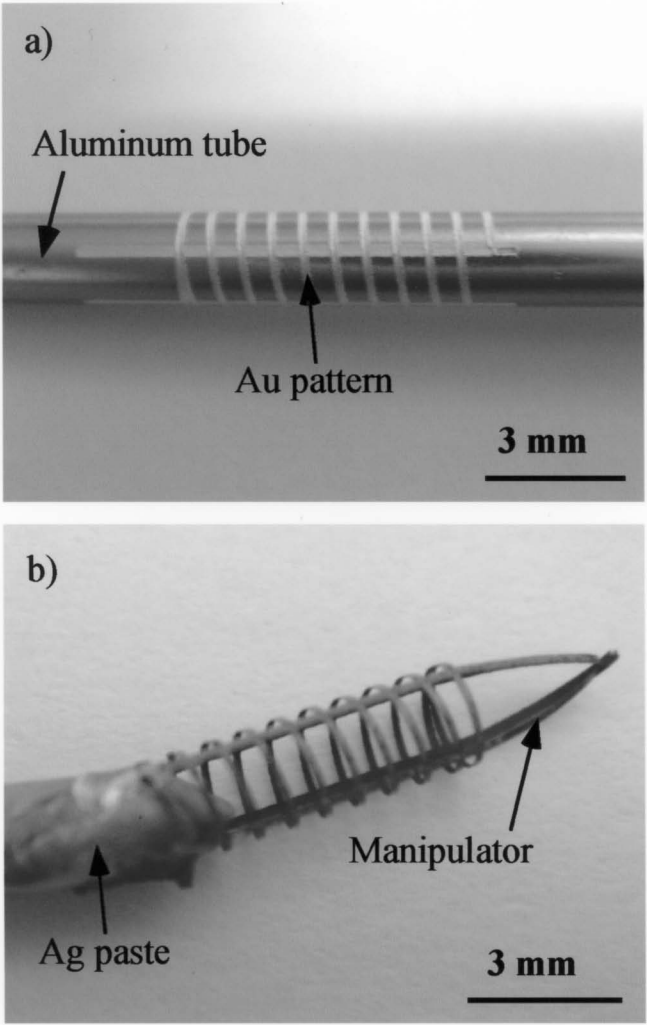

Fig. 7

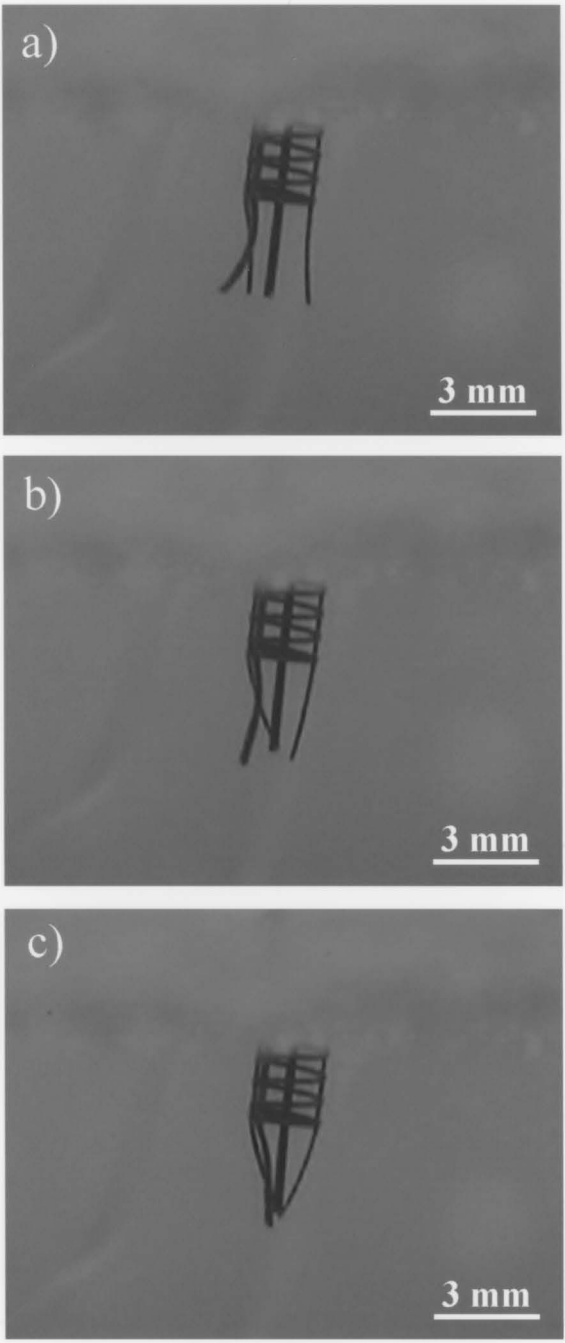

Fig. 8

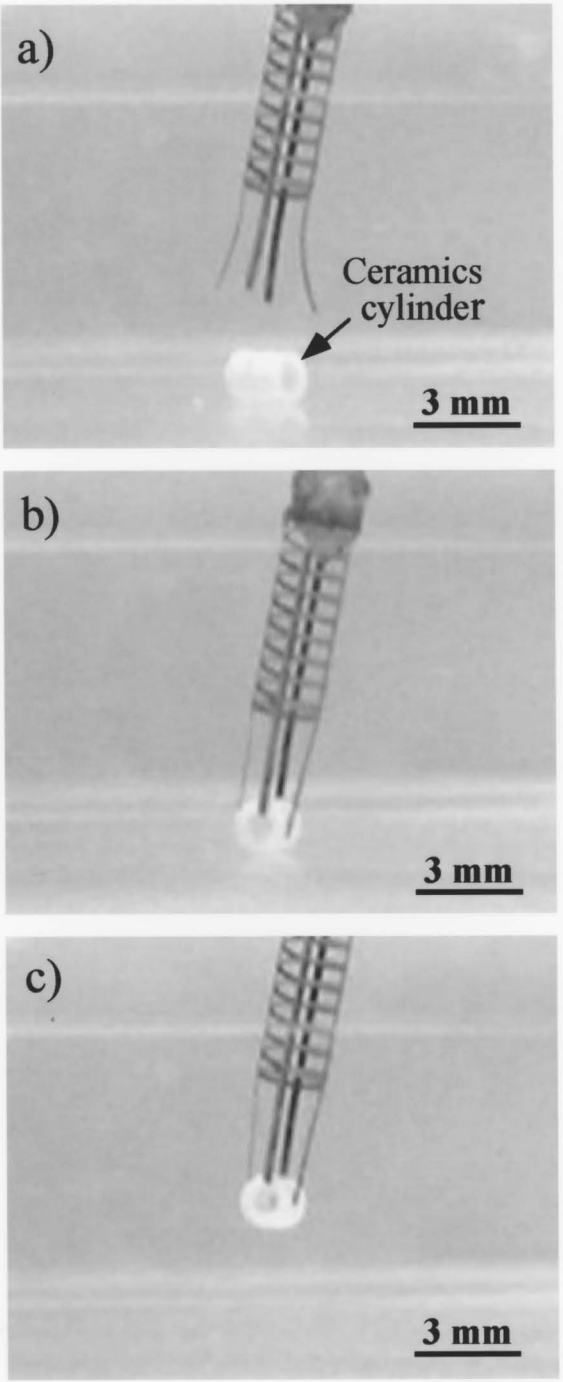

Fig. 9